Electronic Supplementary Information

Mechanistic Insights into On-Surface Reactions from Isothermal Temperature-Programmed X-ray Photoelectron Spectroscopy

Lukas Grossmann[1,2], Manuela Hocke[1], Gianluca Galeotti[2], Giorgio Contini[3], Luca Floreano[4], Albano Cossaro[4], Amit Ghosh[5], Michael Schmittel[5], Johanna Rosen[6], Wolfgang M. Heckl[1,2], Jonas Björk[6]* and Markus Lackinger[1,2]*

[1]Physics Department, Technical University of Munich, James-Franck-Str. 1, 85748 Garching, Germany;

[2]Deutsches Museum, Museumsinsel 1, 80538 Munich, Germany;

[3]Istituto di Struttura della Materia-CNR (ISM-CNR), Via Fosso del Cavaliere 100 and Department of Physics, University of Rome Tor Vergata, Via della Ricerca Scientifica 1, 00133, Roma, Italy;

[4]Istituto Officina dei Materiali Consiglio Nazionale delle Ricerche S.S. 14, km 163.5, Trieste, 34149, Italy;

[5]Center of Micro and Nanochemistry and (Bio)Technology, Organische Chemie I, Universität Siegen, Adolf-Reichwein-Str. 2, 57068 Siegen, Germany;

[6]Linköping University, Department of Physics, Chemistry and Biology, IFM, 581 83 Linköping, Sweden;

* jonas.bjork@liu.se markus@lackinger.org

1. Scanning-Tunneling-Microscopy results

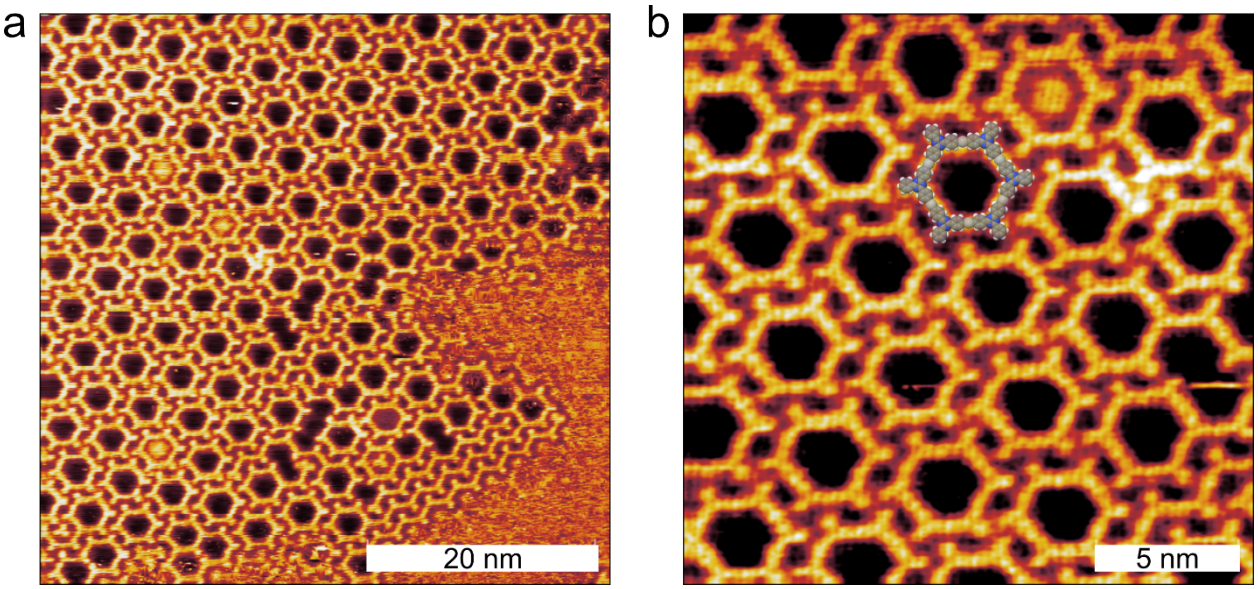

Figure S1. STM images of the organometallic structures observed for **2BPT** on Ag(111). **(a)** overview and **(b)** close up; The structures were prepared by holding the surface temperature at 40 °C for three days. Full debromination of all molecules resulted in organometallic structures with molecules linked by C-Ag-C bonds. The bromine substitution pattern of **2BPT** results in 1D topologies, that is hexagonal rings (as highlighted by the overlay in (b)[1]) or zig-zag chains (e.g. at the lower right in (a)). Despite the prolonged equilibration time, the structures were still comprised of rings as well as curved and straight zig-zag chains (tunneling parameters for (a) and (b): -1.00 V, 50 pA; images were acquired at room temperature).

2. TP-XPS data

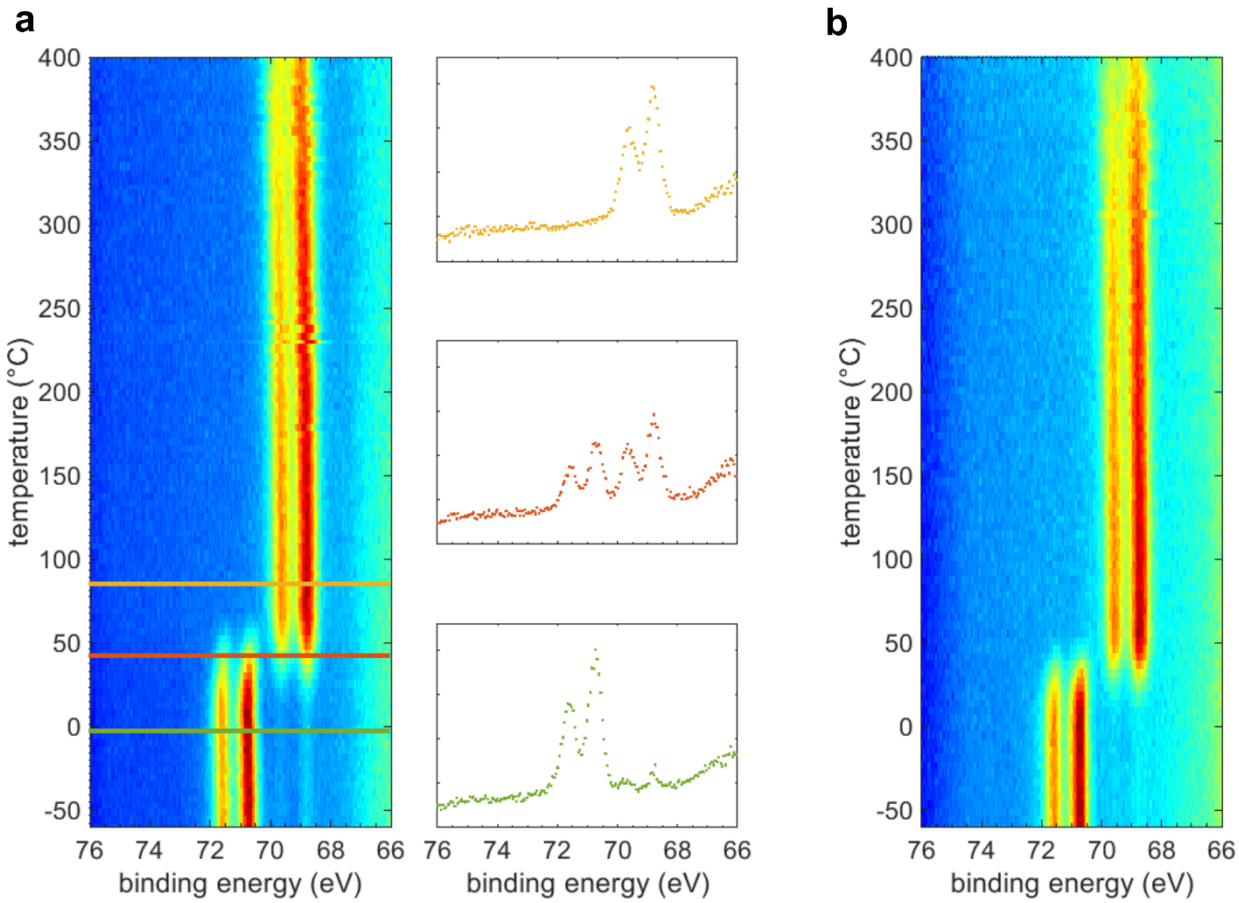

Figure S2 TP-XPS data acquired for the Br 3d core level for **(a) 3BPT** and **(b) 2BPT** on Ag(111) with a linear temperature profile and a heating rate of 0.10 K s^{-1}. From these data the debromination versus temperature traces shown in Figure 1 of the main manuscript were obtained. The right hand side of (a) exemplarily shows XP spectra extracted for fully brominated (bottom, green, -4 °C), partially debrominated (center, red, 42 °C) and fully debrominated (top, orange, 85 °C) molecules. The respective temperatures at which these spectra were acquired are given in parenthesis and are indicated by horizontal lines in the left hand side of (a).

3. Simulation of debromination traces for linear temperature ramps

The debromination traces were computed as concentration of bromine covalently bound to the molecule ($Br_{molecule}$) *versus* time t, but plotted *versus* temperature T. According to the applied linear temperature ramp, the relation between temperature T and time t is given by:

$$T(t) = T_0 + \beta \cdot t$$

with $\beta = 0.10\ K \cdot s^{-1}$ corresponding to the experimental heating rate.

The debromination traces were numerically computed for discrete time steps Δt, where the reaction progression in a single time step was calculated by:

$$N(t + \Delta t) = N(t) + \Delta N(t,\Delta t)$$

We found the simulated traces to converge for time steps of $\Delta t \approx 1s$, but we used time steps of $\Delta t = 0.1\ s$ for a sufficiently large safety margin.

The change of $Br_{molecule}$ concentration $\Delta N(t,\Delta t)$ in a discrete time step Δt is given by:

$$\Delta N(t,\Delta t) = -\ k(T(t)) \cdot N^Z(t) \cdot \Delta t$$

Thereby, $Z = 1$ corresponds to first-order and $Z = 2$ to second-order reaction kinetics, respectively. The dependence of rate constant $k(T(t))$ on the time-dependent temperature $T(t)$ was described by an Arrhenius law:

$$k(T(t)) = A \cdot e^{-\frac{E_a}{k_B \cdot T(t)}}$$

where the pre-exponential A and the activation energy E_a are the free parameters for the fit. Accordingly, the grid searches (Figure 1 of the main manuscript and Figures S9) were performed in this two-dimensional parameter space.

Extension 1: Different activation energies

To consider our DFT results for the debromination of 3BPT, we implemented a model with two different activation energies: E_{a1} corresponds to the activation energy for the 1st debromination of a 3BPT molecule, while a similar activation energy $E_{a2} = E_{a3}$ was used for the 2nd and 3rd debromination reaction according to the DFT results (see Figure 3 of main manuscript). This extension also requires separate accounting of the three distinct reaction sites N_1, N_2, and N_3, where the index refers to the three different bromine substituents of a **3BPT** molecule. The total amount of brominated sites N_{total} as measured by TP-XPS is given by:

$$N_{total}=N_1+N_2+N_3$$

To compare experimental and simulated curves, N_{total} was normalized to unity for the unreacted state. The simulation was performed analogously to the previous model, but independently for the different reaction sites:

$$\Delta N_1(t,\Delta t) = -k_1(T(t))\cdot N_1^z(t)\cdot \Delta t$$

$$\Delta N_2(t,\Delta t) = -k_2(T(t))\cdot N_2^z(t)\cdot \Delta t$$

$$\Delta N_3(t,\Delta t) = -k_3(T(t))\cdot N_3^z(t)\cdot \Delta t$$

We restricted the grid search to a second-order rate law with $Z=2$. The different activation energies give rise to different rate constants k_1, k_2, and k_3, whose temperature dependence is also described by an Arrhenius law:

$$k_1(T(t)) = A\cdot e^{-\frac{E_{a1}}{k_B\cdot T(t)}};\quad k_2(T(t)) = A\cdot e^{-\frac{E_{a2}}{k_B\cdot T(t)}};\quad k_3(T(t)) = A\cdot e^{-\frac{E_{a3}}{k_B\cdot T(t)}};$$

As indicated, we used a common pre-exponential $A=A_1=A_2=A_3$,
which for $E_{a2}=E_{a3}$ implies $k_2(T(t))=k_3(T(t))$.

Extension 2: Including Ag adatoms

The second-order rate law with identical reactants, i.e. with $Z=2$, allowed a straightforward evaluation of the appropriateness of a higher order reaction kinetics. However, for the proposed Ag adatom-activated debromination the reaction rate is actually proportional to the product of the concentrations of brominated sites N_{Br} and Ag adatoms N_{Ag}:

$$\Delta N_{Br}(t,\Delta t) = -k(T(t))\cdot N_{Br}(t)\cdot N_{Ag}(t)\cdot \Delta t,$$

where the temperature dependence of the rate constant $k(T(t))$ was described by the usual Arrhenius law. To keep the number of free parameters at a minimum, we restrict the model to reactions where one Ag adatom is consumed by each debromination. Accordingly, the changes in the concentrations of brominated sites and Ag adatoms are identical for each time step:

$$\Delta N_{Br}(t,\Delta t) = \Delta N_{Ag}(t,\Delta t),$$

In this model, the concentration of available Ag adatoms at the beginning of the reaction $N_{Ag,0}=N_{Ag}(t=0)$ relative to the initial amount of brominated sites $N_{Br,0}=N_{Br}(t=0)$ represents a new fit parameter ($N_{Ag,0}$:$N_{Br,0}$). We implicitly assume $N_{Ag,0}>N_{Br,0}$, because otherwise the reaction would not run to completion as observed experimentally. The

influence of processes providing new Ag adatoms is neglected for the possible case $N_{Ag,0} < N_{Br,0}$, which implies that the amount of initially available Ag adatoms is completely consumed in the course of the reaction.

4. Additional grid search results

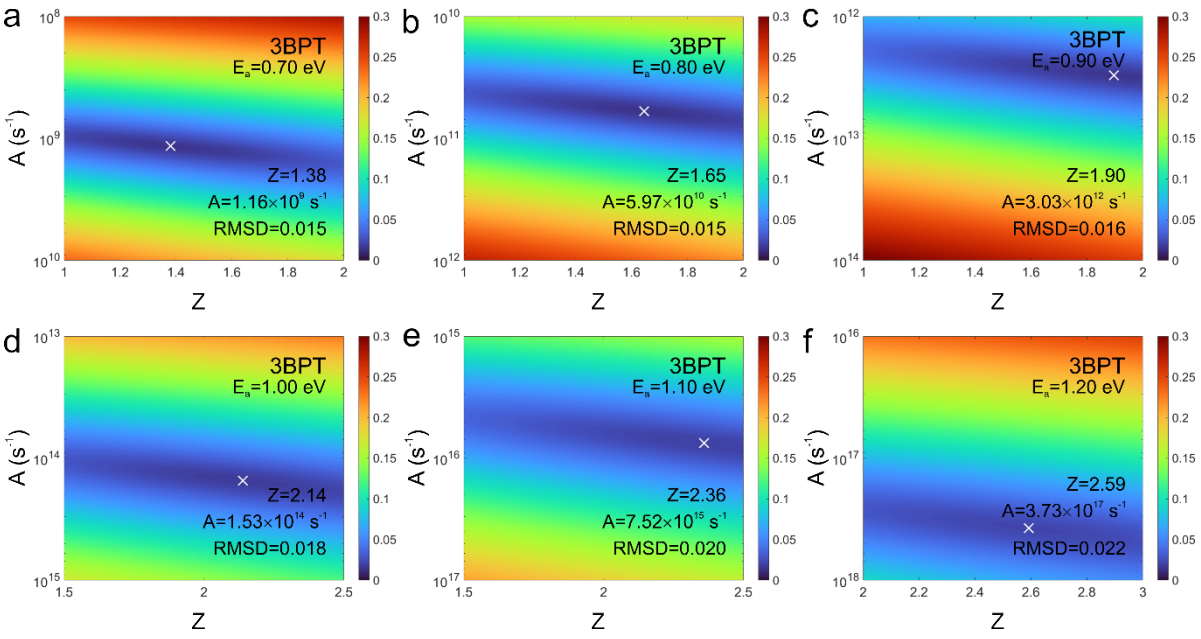

Figure S3 Grid searches (300×300 points) for optimization of the fitting parameters reaction order Z and pre-exponential A on a logarithmic axis. The plots refer to the debromination of **3BPT**. For each individual grid search the activation energy was kept fixed at **(a)** $E_a = 0.70\ eV$, **(b)** $E_a = 0.80\ eV$, **(c)** $E_a = 0.90\ eV$, **(d)** $E_a = 1.00\ eV$, **(e)** $E_a = 1.10\ eV$, and **(f)** $E_a = 1.20\ eV$ as indicated. The color coding represents the RMSD between experimental and computed traces. The white crosses mark the optimal combination of fit parameters. The corresponding values of the fit parameters and the resulting minimum RMSD are indicated. As expected higher E_a result in higher A. However, another trend becomes apparent: Higher activation energies E_a always lead to higher reaction orders Z.

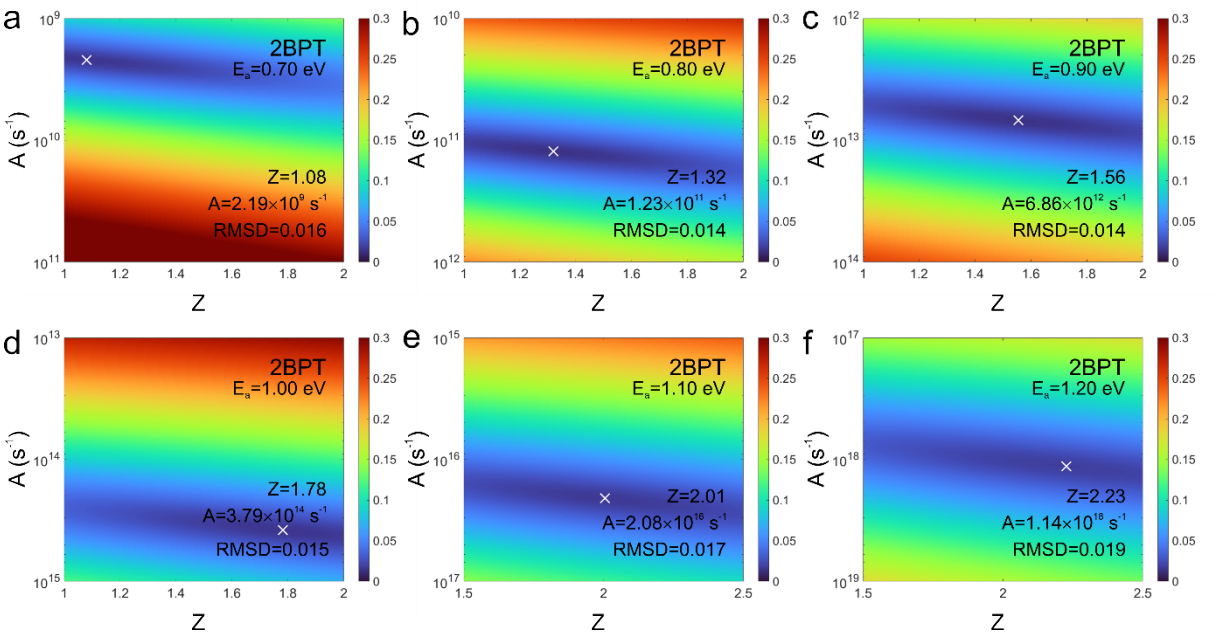

Figure S4 Grid searches (300×300 points) for optimization of the fitting parameters reaction order Z and pre-exponential A on a logarithmic axis. The plots refer to the debromination of **2BPT**. For each individual grid search the activation energy was kept fixed at **(a)** $E_a = 0.70\ eV$, **(b)** $E_a = 0.80\ eV$, **(c)** $E_a = 0.90\ eV$, **(d)** $E_a = 1.00\ eV$, **(e)** $E_a = 1.10\ eV$, and **(f)** $E_a = 1.20\ eV$ as indicated. The color coding represents the RMSD between experimental and computed traces. The white crosses mark the optimal combination of fit parameters. The corresponding values of the fit parameters and the resulting minimum RMSD are indicated. As expected higher E_a result in higher A. However, another trend becomes apparent. Higher activation energies E_a always lead to higher reaction orders Z. These grid searches demonstrate that a single best value for the reaction order cannot be stated as it also depends on the concrete choice of the other fit parameters. Equally good fits can be obtained for an appropriate combination of Z, E_a and A. In comparison to **3BPT** (Figure S3), optimization for **2BPT** yields lower reaction orders Z but higher pre-exponentials A for a given activation energy E_a.

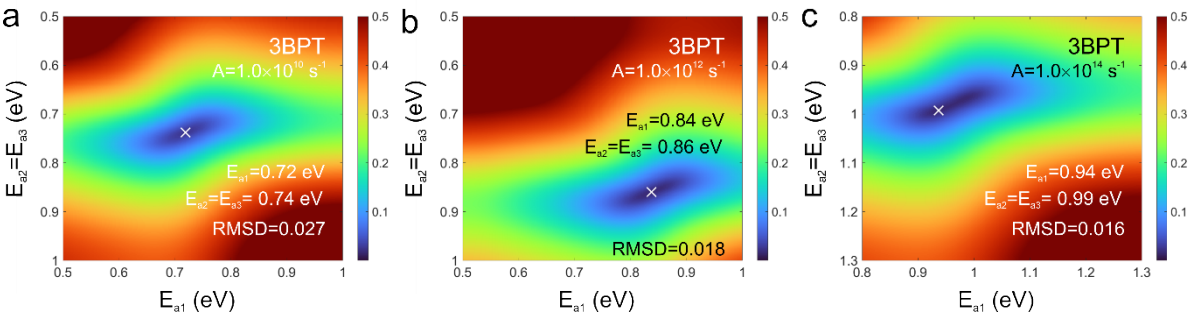

Figure S5 Grid search (300×300 points) for optimization of the fitting parameters activation energy for the first debromination E_{a1} and activation energies for the second and third debromination $E_{a2} = E_{a3}$. The plots refer to the debromination of **3BPT** modelled with **second-order** reaction kinetics. A common pre-exponential was used and kept fixed at **(a)** $A = 1.0 \cdot 10^{10} s^{-1}$, **(b)** $A = 1.0 \cdot 10^{12} s^{-1}$, and **(c)** $A = 1.0 \cdot 10^{14}\, s^{-1}$ as indicated. The color coding represents the RMSD between experimental and computed traces. The white crosses mark the optimal combination of fit parameters. The corresponding values of the fit parameters and the resulting minimum RMSD are indicated. This model takes into account the DFT calculations for the Ag adatom-activated debromination of **3BPT**, which yielded a higher activation energy for the first debromination of $E_{a1} = 0.80\, eV$, while the activation energies for the second and third debrominations of $E_{a2} = 0.66\, eV$ and of $E_{a3} = 0.70\, eV$ were both lower and fairly similar. However, this difference in calculated activation energies is not reflected in the fitting results where the optimized values for E_{a1} and $E_{a2} = E_{a3}$ are similar. The actual difference increases monotonically with the pre-exponential A, but remains less than $50\, meV$.

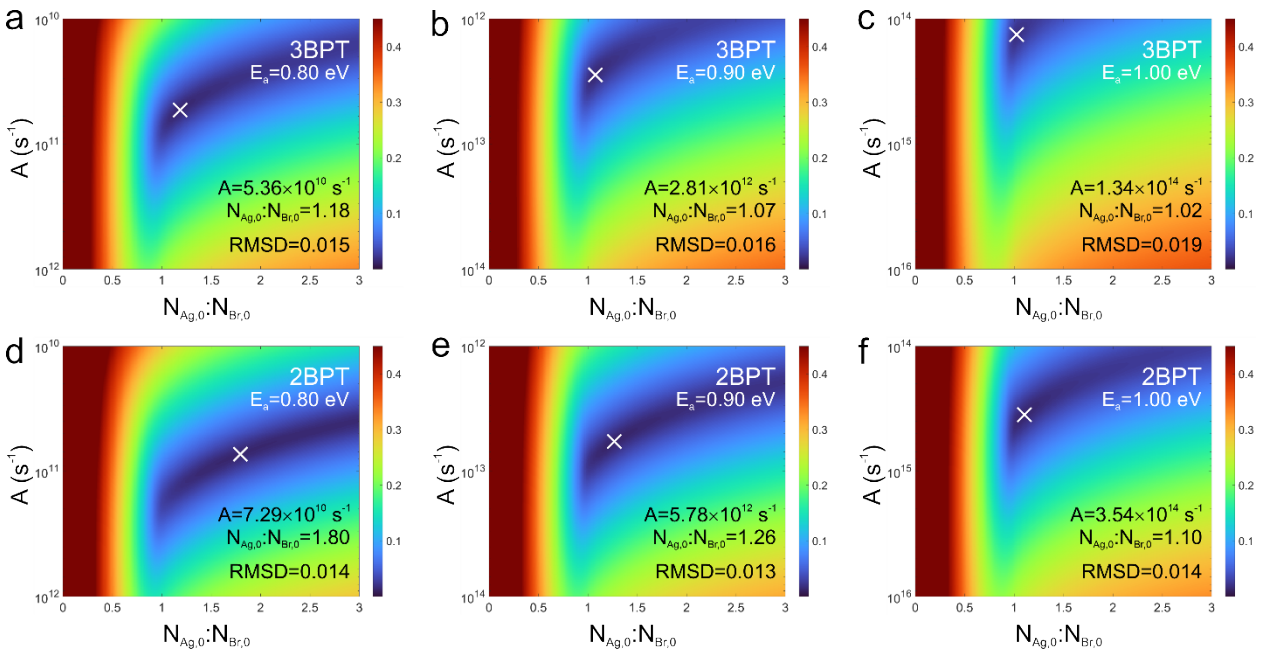

Figure S6 Fitting debromination versus temperature traces with Ag adatom model. Additional grid searches (300×300 points) for optimization of the fitting parameters pre-exponential A and the initial ratio of Ag adatoms to brominated sites $N_{Ag,0}$:$N_{Br,0}$ for **(a)** – **(c) 3BPT** and **(d)** – **(f) 2BPT**. Note that A is plotted on a logarithmic axis. Analogous to Figures 5(a) and (b) of the main manuscript the activation energy was kept fixed at (a) / (d) $E_a = 0.80\ eV$, (b) / (e) $E_a = 0.90\ eV$ and (c) / (f) $E_a = 1.00\ eV$ as indicated. The color coding represents the RMSD between experimental and computed traces. The white crosses mark the optimal combination of fit parameters. The corresponding values of the fit parameters and the resulting minimum RMSD are indicated. As expected higher E_a also result in higher A. However, the pre-exponentials obtained for **3BPT** and **2BPT** are now much closer than for second-order reaction kinetics with identical reactants (see Figure S9). Further trends can be identified: Higher activation energies yield lower values $N_{Ag,0}$:$N_{Br,0}$ for both **2BPT** and **3BPT**. But for a given E_a a higher value for $N_{Ag,0}$:$N_{Br,0}$ is consistently obtained for **2BPT**.

5. Fitting of debromination traces *versus* time at constant temperature

Individual time traces were extracted from the complete time course of the debromination acquired for a stepped temperature-profile for the segments with constant temperature (Figure 2 of main manuscript). For both **3BPT** and **2BPT** each trace was fitted with the analytical expression of the time course according to the respective rate law:

First-order reaction kinetics: $N(t) = N_0 \cdot e^{-k(T) \cdot t}$ (S1)

Second-order reaction kinetics: $\frac{1}{N(t)} = \frac{1}{N_0} + k(T) \cdot t \rightarrow N(t) = \frac{1}{\frac{1}{N_0} + k(T) \cdot t}$ (S2)

Irrespective of reaction order, the two fitting parameters are $N_0 = N(t = 0)$, that is the concentration of unreacted, still brominated sites at the beginning of the trace for $t = 0$, and the temperature dependent rate constant $k(T)$. Exemplary fitting results obtained for both reaction orders are depicted in Figure S7, also clearly visualizing that the fitting curves for both first- and second-order almost coincide and are virtually indistinguishable. From this we conclude that in view of the scatter of experimental data, it is impossible to discriminate between first- and second-order reaction kinetics solely based on these time traces. Fitting of all time traces for both molecules with either first- or second-order kinetics afforded the data sets of rate constant $k(T)$ *versus* temperature summarized in Table 1.

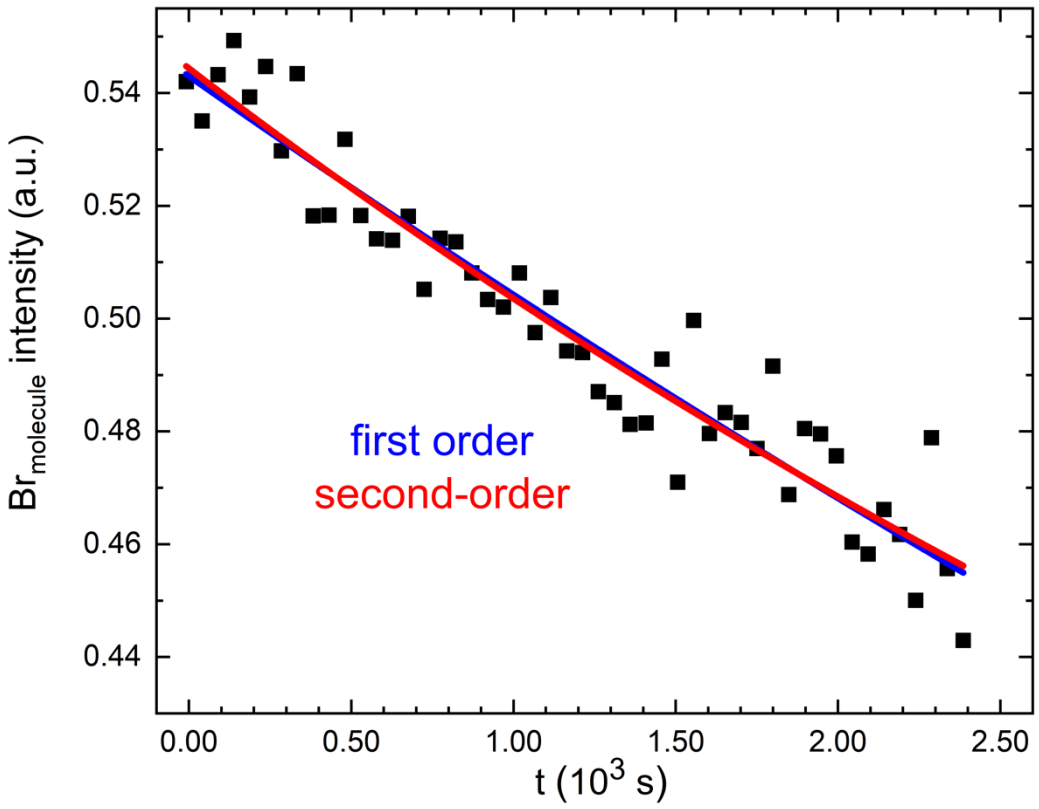

Figure S7. Example of fitting of the time traces. Here, the trace acquired for **2BPT** at 15 °C is exemplarily shown. It was recorded in the initial phase of the debromination for about 50 minutes. Blue and red curves show the fitted time traces obtained for assuming either first- or second-order reaction kinetics based on equations (S1) and (S2), respectively. Along the entire length of the time trace the two curves virtually coincide with differences being markedly smaller than the scatter of experimental data points. From this we conclude that it is extremely challenging, if not impossible to infer the reaction order of the debromination from the experimentally measured time course of the turnover at constant temperature.

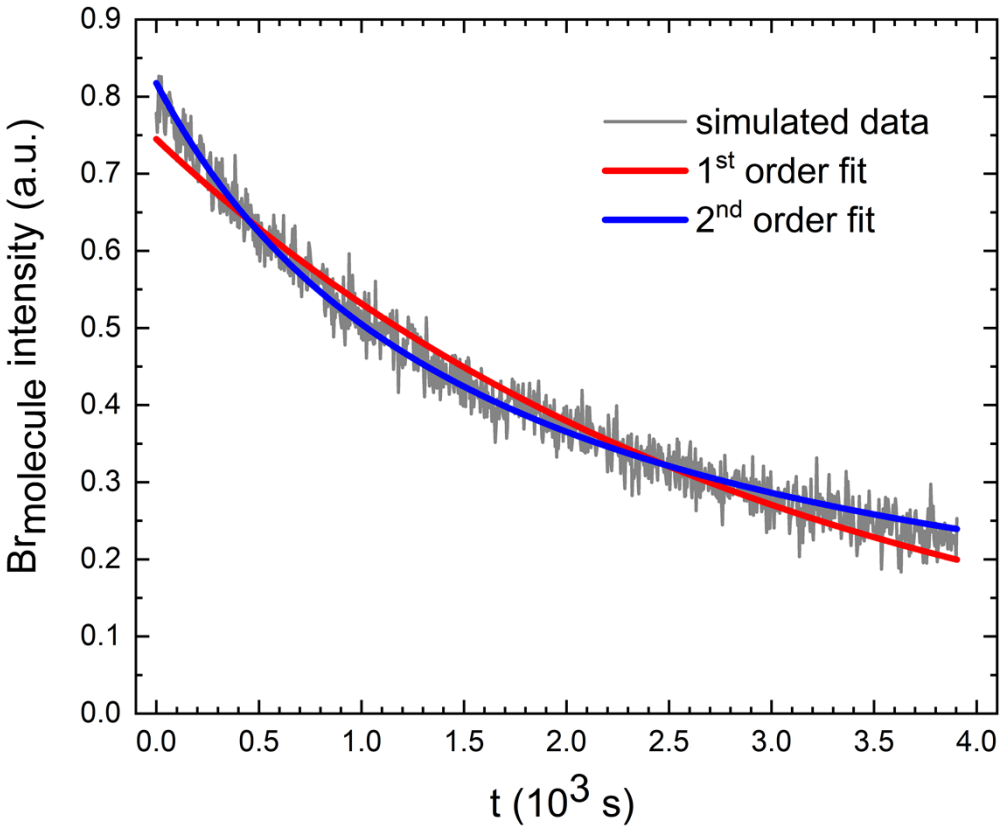

Figure S8. Demonstration of the fitting ambiguity in the Ag adatom model. The gray line represents a numerically simulated debromination *versus* time trace for **3BPT** at constant temperature of 15 °C with an activation energy of $E_a = 0.80\ eV$, a pre-exponential of $A = 5.36 \cdot 10^{10} s^{-1}$, and an initial ratio of Ag adatoms to brominated sites of $N_{Ag,0}{:}N_{Br,0} = 1.18$ (cf. Figure S6(a)). To account for the experimental error, the simulated curve was superimposed with 5% Gaussian white noise. Fitting with both the analytical functions for first-order ($R^2 = 0.97$) and second-order ($R^2 = 0.98$) reaction kinetics according to equations (S1) and (S2), respectively, gives satisfactory agreement with the corresponding R^2 values given in parentheses. From this we conclude that the shape of even extended time traces does not necessarily allow unambiguous inference of the reaction order, which may also not be an integer for more complex reaction scenarios.

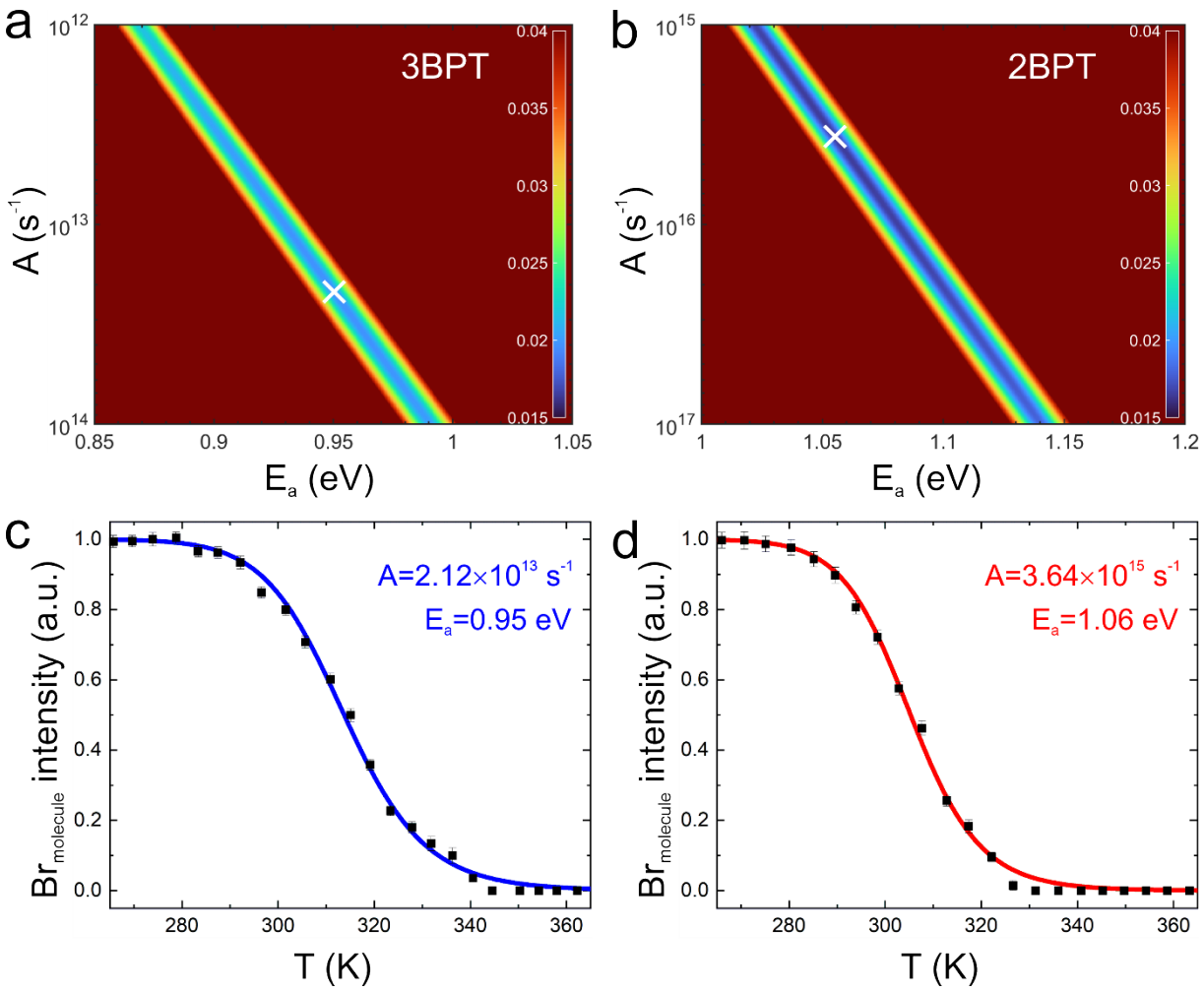

Figure S9. Grid search (400×400 points) for fit parameters assuming a **second-order** kinetics for **(a) 3BPT** and **(b) 2BPT**. Analogous to first-order kinetics, a single best fit is not obtained for a unique-point in this two-dimensional parameter space. Comparably good fits can be obtained along lines (show in dark blue), that is for a linear combination of E_a and $ln(A)$. Both fits also exhibit a weakly pronounced global minimum as indicated by the white crosses. Yet, in contrast to first-order reaction kinetics, the activation energies of $0.95\ eV$ (**3BPT**) and $1.06\ eV$ (**2BPT**) and pre-exponentials of $2.12 \cdot 10^{13} s^{-1}$ (**3BPT**) and $3.65 \cdot 10^{15} s^{-1}$ (**2BPT**) appear more sensible. The corresponding simulated (solid lines) and experimental (squares) debromination *versus* temperature traces match well for both **(c) 3BPT** and **(d) 2BPT**. In summary, second-order reaction kinetics provides a consistent description of debromination on Ag(111).

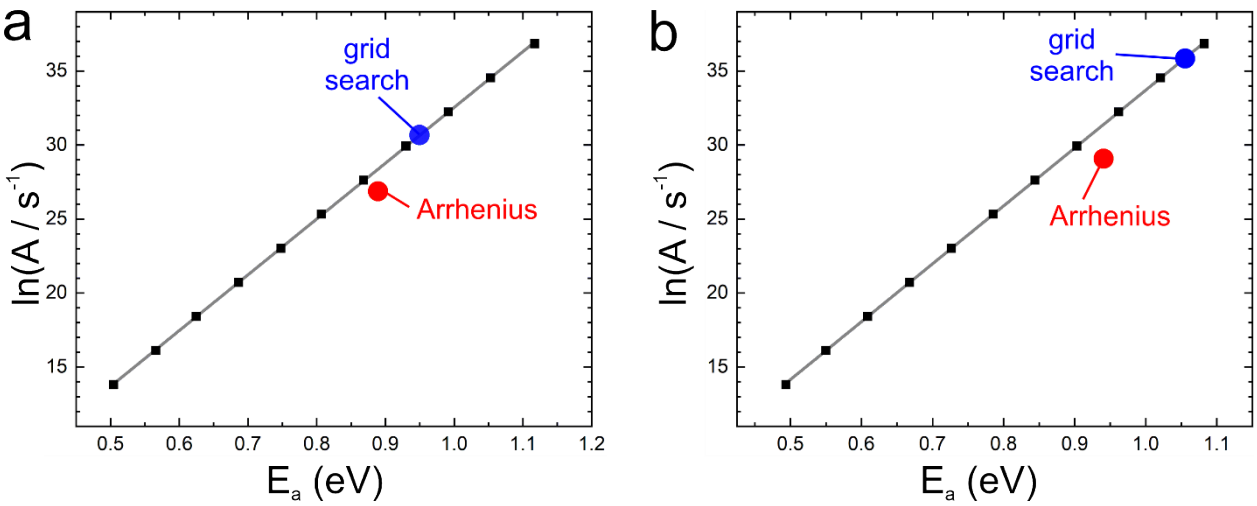

Figure S10. Consistency test between TP-XPS with linear and stepped temperature profiles evaluated for **second-order** reaction kinetics. The plots show the optimized fitting parameters (solid squares) along the valley of minima for **(a) 3BPT** and **(b) 2BPT**. The data points were derived by setting the pre-exponential A to a fixed value (in decadic logarithmic scale) and optimizing the activation energy E_a. The solid grey lines represent linear fits. The combinations of $ln(A)$ and corresponding E_a perfectly lie on a straight line, that is the valley of minima. The blue circles on the lines represent the weakly pronounced global minima as identified in the corresponding grid searches (Figure 1 of main manuscript). The red circles represent the E_a and $ln(A)$ obtained from the Arrhenius plots for second-order (Figure 2 of main manuscript). Even though the two different optima do not fully coincide, the close proximity of the kinetic parameters derived from TP-XPS with linear and stepped shows a reasonable level of consistency between the two distinct experimental approaches.

Table S1. Summary of rate constants $k(T)$ (in s^{-1}) as obtained from fitting the isothermal time traces with the analytical functions for either first- or second-order kinetics. Fitting errors are stated in parenthesis.

	3BPT		**2BPT**	
	1st order	2nd order	1st order	2nd order
15 °C	7.74×10^{-5} (2.68×10^{-6})	1.31×10^{-4} (4.42×10^{-6})	7.41×10^{-5} (3.23×10^{-6})	1.49×10^{-4} (6.43×10^{-6})
20 °C	7.93×10^{-5} (8.22×10^{-6})	2.16×10^{-4} (2.22×10^{-5})	8.51×10^{-5} (1.13×10^{-5})	2.19×10^{-4} (2.87×10^{-5})
25 °C	1.18×10^{-4} (1.16×10^{-5})	4.09×10^{-4} (3.98×10^{-5})	1.72×10^{-4} (1.13×10^{-5})	5.89×10^{-4} (3.98×10^{-5})
30 °C	1.56×10^{-4} (1.19×10^{-5})	7.26×10^{-4} (5.46×10^{-5})	1.96×10^{-4} (1.53×10^{-5})	9.04×10^{-4} (7.05×10^{-5})
35 °C	2.45×10^{-4} (3.13×10^{-5})	16.5×10^{-4} (2.21×10^{-4})	3.67×10^{-4} (2.48×10^{-4})	46.8×10^{-4} (31.4×10^{-4})

6. Additional DFT results

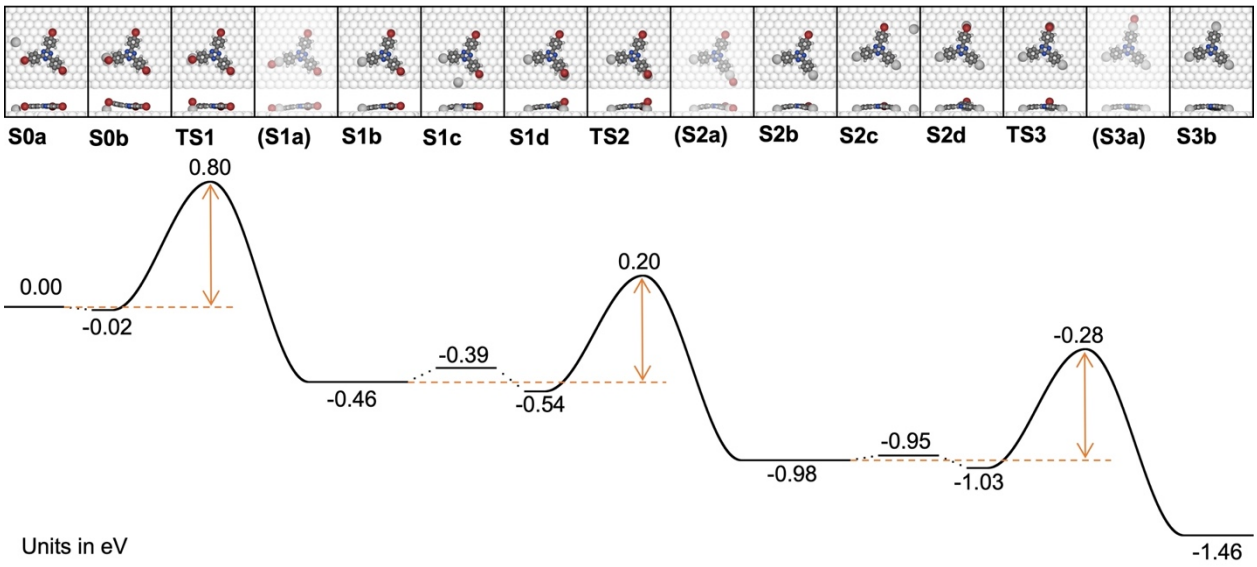

Figure S11. Complete energy profile and corresponding structures for the Ag adatom-activated debromination of **3BPT** on Ag(111). Here, the energies of all intermediate structures are indicated, with exception of those where the bromine atoms are bonded to the Ag adatom (why these structures are shown dimmer). The orange dashed lines and double headed arrows indicate how the activation energies shown in Figure 3 of the main manuscript were calculated according to equation (1).

7. Synthesis

The synthesis and characterization of **3BPT** was previously described.[2]

Synthesis and characterization of 2BPT

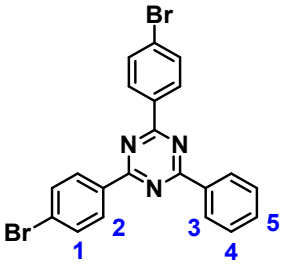

2BPT

Benzoyl chloride (1.55 g, 11.0 mmol) and 4-bromobenzonitrile (4.00 g, 22.0 mmol) was mixed in 15 mL of dichloromethane and cooled at 0 °C in an ice-bath and stirred for 30 min. Then antimony chloride (3.30 g, 11.0 mmol) was added dropwise to the solution. The mixture was stirred at room temperature for one hour and further refluxed for overnight. The cold mixture was filtrated and the collected yellow solid was washed with dichloromethane. The solid was slowly added to 100 mL of ice-cold ammonia solution and stirred for 30 min at 0 °C. Then the mixture was stirred for 4 h at room temperature. Subsequently, the mixture was filtrated and washed with water. Thereafter, the white solid was added to 30 mL of N,N′-dimethylformamide and heated at 155 °C for 30 min. The insoluble solid was separated by filtration. Heating and filtration was repeated three times. Then it was dried under vacuum, and 2,4-bis(4-bromophenyl)-6-phenyl-1,3,5-triazine (**2BPT**) was obtained as a colorless solid (2.05 g, 4.39 mmol, 40%). ^{1}H NMR ($CDCl_3$, 400 MHz): δ = 8.72 (m, 2H, 3-H), 8.61 (d, 3J = 8.8 Hz, 4H, 2-H), 7.70 (d, ^{3}J = 8.8 Hz, 4H, 1-H), 7.60 (m, 3H, 4 + 5-H); ^{13}C NMR ($CDCl_3$, 400 MHz): δ = 171.3, 170.4, 135.2, 134.4, 132.2, 131.4, 130.0, 128.4, 128.1, 127.1. ESI-MS: Calculated *m*/*z* (%) = 468.0 (100). Found *m*/*z* (%) = 468.9 (100). Elemental analysis: [$C_{21}H_{13}Br_2N_3(3H_2O)$]: Calculated, C, 53.37; H, 2.90; N, 8.89. Found, C, 53.06; H, 2.62; N, 8.77.

^{1}H and ^{13}C NMR spectra

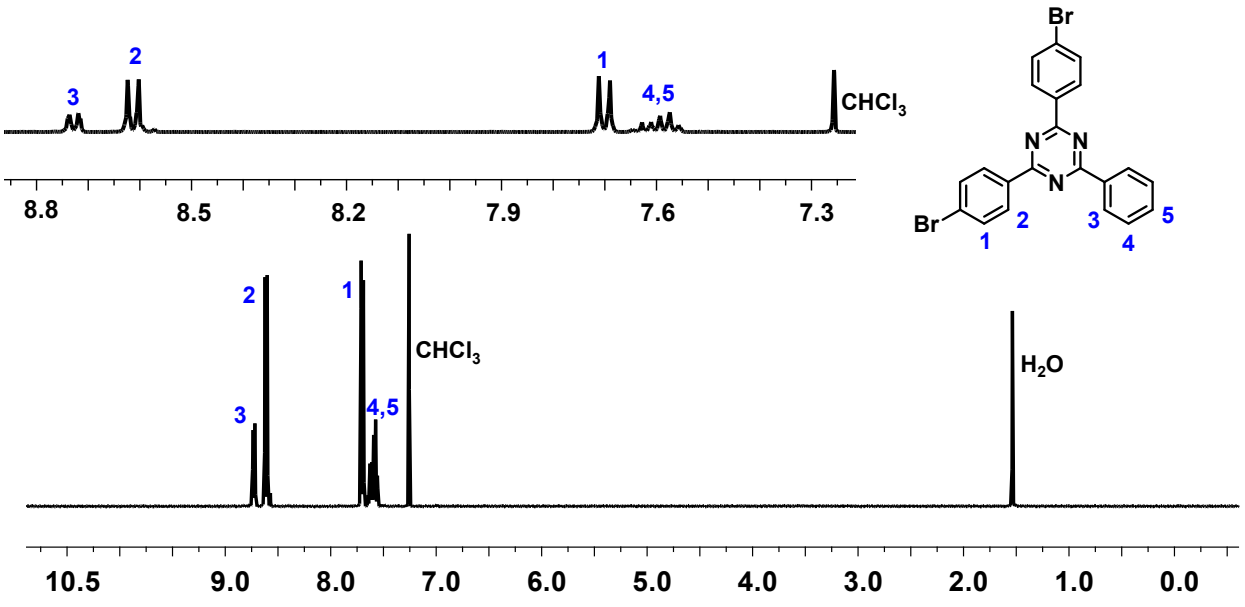

Figure S12 ^{1}H NMR spectrum of **2BPT** ($CDCl_3$, 400 MHz).

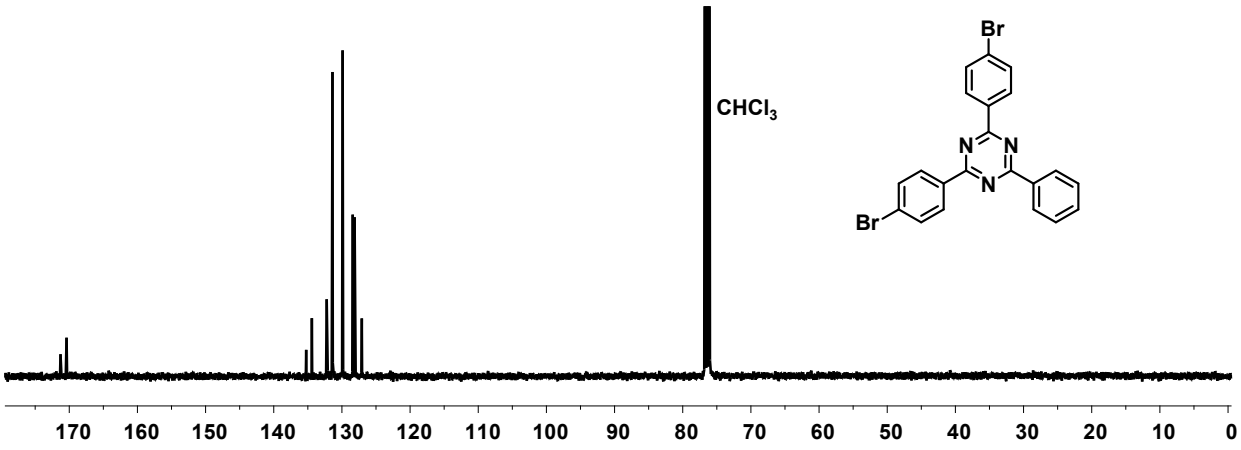

Figure S13 ^{13}C NMR spectrum of 2BPT ($CDCl_3$, 100 MHz).

ESI-MS spectra

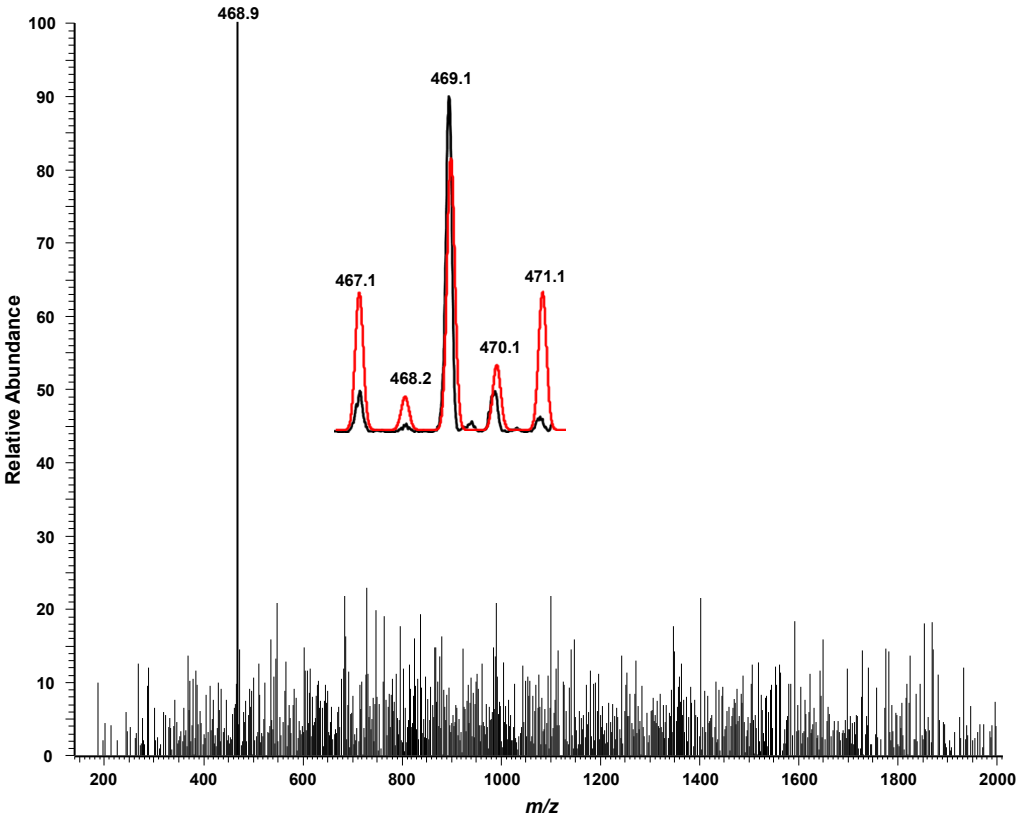

Figure S14 ESI-MS of **2BPT** in CH_2Cl_2.

8. References

(1) Hanwell, M. D.; Curtis, D. E.; Lonie, D. C.; Vandermeersch, T.; Zurek, E.; Hutchison, G. R. Avogadro: an advanced semantic chemical editor, visualization, and analysis platform. *J. Cheminformatics* **2012**, *4*, 17.

(2) Grossmann, L.; Duncan, D. A.; Jarvis, S. P.; Jones, R. G.; De, S.; Rosen, J.; Schmittel, M.; Heckl, W. M.; Björk, J.; Lackinger, M. Evolution of adsorption heights in the on-surface synthesis and decoupling of covalent organic networks on Ag(111) by normal-incidence X-ray standing wave. *Nanoscale Horiz* **2021**, *7* (1), 51-62.